

Evolution of QPO During Discovery Outburst of MAXI J1834-021: Estimation of Intrinsic Parameters from Spectro-Temporal Study

DIPAK DEBNATH^{1,2} AND HSIANG-KUANG CHANG^{1,3}

¹*Institute of Astronomy, National Tsing Hua University, Hsinchu 300044, Taiwan*

²*Institute of Astronomy Space and Earth Science, P 177, CIT Road, Scheme 7m, Kolkata 700054, India*

³*Department of Physics, National Tsing Hua University, Hsinchu 300044, Taiwan*

Submitted to ApJ

ABSTRACT

The Galactic transient black hole candidate (BHC) MAXI J1834-021 was detected for the first time by MAXI/GSC on February 05, 2023 and it was active for next ~ 10 months. A monotonic evolution of low-frequency QPOs from higher to lower frequencies is observed in the middle-phase of the outburst. We study this evolution of the QPO with the propagating oscillatory shock (POS) model, and it suggests the presence of a receding shock. The POS model fit also estimates the mass of the source to be $12.1 \pm 0.3 M_{\odot}$. We also study the broadband (0.5-70 keV) nature of the source using archival data of NICER and NuSTAR on March 10, 2023 with the both phenomenological (combined disk blackbody plus powerlaw) and physical (*nthComp*, *kerrbb*, *TCAF*) models. The mass of the BHC estimated by the *kerbb* and *TCAF* models is found to be consistent with POS model fits as well as reported in our recent work. Combining all these methods, we predict mass of the source as $12.3^{+1.1}_{-2.0} M_{\odot}$. The *kerbb* model fit also estimates the spin, distance, and inclination of the source to be $0.13^{+0.03}_{-0.02}$, $9.2^{+0.4}_{-0.9}$ kpc, and $80^{\circ} 0^{+2.7}_{-6.0}$, respectively. The combined spectral study suggests harder spectral state of the source with a higher dominance of the sub-Keplerian halo accretion rate over the Keplerian disk rate. The consistency of the observed frequency of the QPO with that of obtained from the *TCAF* model fitted shock parameters, confirms shock oscillation as the origin of the QPO.

Keywords: X-ray binary stars(1811) – X-ray transient sources(1852) – Black holes(162) – Black hole physics(159) – Accretion(14) – Shocks (2086)

1. INTRODUCTION

The black hole (BH) continuum spectrum mainly consists of two components: thermal multi-color disk blackbody (DBB) and non-thermal power-law (PL) components. In addition to ionized line emissions, strong reflection features from ionized plasma are sometimes observed in the BH spectrum. To understand physics of accretion processes around the BHs, one needs to perform a detailed study of the spectral and temporal properties of the sources using physical accretion disk models. These models provide a clear understanding about the flow dynamics of BH X-ray binaries during their active phases. *nthComp* (Zdziarski et al. 1996; Zycki et al. 1999), *kerrbb* (Li et al. 2005), *pexrav* (Magdziarz et al. 1995), *relxill* (Garcia et al. 2014, and references

therein), and *TCAF* (Chakrabarti & Titarchuk 1995; Debnath et al. 2014, 2015) are some of the widely used physical models. The *nthComp* model is used to understand nonthermal Comptonized flux contributions and its high-energy roll-over, while the *kerrbb* model is a multi-temperature blackbody model for a thin relativistic accretion disk around a Kerr BH. The *pexrav* model describes an exponentially cut-off power-law spectrum reflected from neutral material, such as Fe and Ni, while *relxill* model is a relativistic accretion disk model that effectively explains the reflection features observed in BHs. The *TCAF* model considers two types of accretion flows: a Keplerian disk (high viscosity, high angular momentum, geometrically thin, and optically thick) and a sub-Keplerian halo (low viscosity, low angular momentum, geometrically thick, and optically thin) to explain the physical processes around BHs. These physical models also provide reliable estimates of intrinsic source parameters such as mass, spin, distance, and inclination angle.

In general, four spectral states—hard (HS), hard-intermediate (HIMS), soft-intermediate (SIMS), and soft (SS)—are observed during the outburst of a transient black hole candidate (BHC). These states are classified based on their distinct spectral and temporal properties (Remillard & McClintock 2006; Belloni et al. 2005; Nandi et al. 2012). Low-frequency (0.01–30 Hz) quasi-periodic oscillations (LFQPOs) are a characteristic temporal feature commonly observed during the hard and intermediate spectral states of transient BHCs. Based on their properties (centroid frequency, quality factor or Q-value, rms amplitude, noise characteristics, time lag, etc.), LFQPOs are categorized into three types: A, B, and C (Casella et al. 2005). Typically, type-C QPOs are observed to evolve monotonically during the HS and HIMS states in both the rising and declining phases of an outburst (Nandi et al. 2012; Debnath et al. 2013). In contrast, type-B and type-A QPOs are sporadically detected during the SIMS spectral state. According to the shock oscillation model (SOM) introduced by Chakrabarti and his collaborators (Molteni et al. 1996; Ryu et al. 1997), LFQPOs originate due to oscillations of the shock. In the TCAF solution (Chakrabarti & Titarchuk 1995), a hot Comptonizing region, known as ‘CENBOL’, naturally forms during the accretion process in the post-shock region. In the SOM framework, shock oscillations occur due to the heating and cooling effects within the CENBOL. The model suggests that sharp type-C QPOs arise from resonance oscillations of the shock, while type-B QPOs occur either due to the non-satisfaction of the Rankine-Hugoniot condition or due to a weakly resonating CENBOL. The broader type-A QPOs are attributed to weak oscillations of the shockless centrifugal barrier (see Chakrabarti et al. 2015). To explain the evolution of QPO frequencies during the rising and declining harder spectral states of transient BHCs, a time-varying form of the SOM, namely the propagating oscillatory shock (POS) model, was introduced in 2005 (see Chakrabarti et al. 2005, 2008).

The Galactic ‘faint’ transient BHC MAXI J1834–021 was first detected by MAXI/GSC (Negoro et al. 2023) on February 05, 2023 (MJD 59980). Unfortunately, it was reported nearly a month later, on 2023 March 6 (MJD 60009). Based on the source flux observed from February 28, 2023 (MJD 60003.95) to March 1, 2023 (MJD 60004.53), Negoro et al. (2023) estimated the source location as (RA, Dec) = (278°.634, –2°.130) = (18^h34^m32^s, –02°07′47″) (J2000) with a 90% confidence level. The maximum average flux of the source during the aforementioned period was observed to be 18 ± 4 mCrab in the 4–10 keV MAXI/GSC band, with a 1σ error. Subsequently, MAXI J1834–021 was monitored in multiple wavelength bands, including X-rays (Swift, NICER, NuSTAR; see Kennea et al. 2023; Marino et al. 2023; Homan et al. 2023), and optical (LCO and Faulkes telescopes; see Saikia et al. 2023). The source was not detected in the 15.5 GHz band by the AMI-LA radio

telescope (Bright et al. 2023). Based on preliminary spectral and temporal analyses, including the detection of LFQPOs using NICER data, Homan et al. (2023) confirmed the source as a black hole low-mass X-ray binary.

In Debnath & Chang (2025, hereafter Paper-I), detailed spectral and temporal studies of MAXI J1834–021 has been done to understand accretion flow properties of the source during its entire 2023 active phase using NICER data. The study suggests that it showed double ‘failed’ outbursts during its 2023 epoch. The spectral study using both phenomenological (combined disk blackbody plus powerlaw) and physical (TCAF) models show a strong dominance of nonthermal photons from ‘hot’ Compton cloud throughout the 2023 active phase. During entire active phases, only harder spectral states are observed. The TCAF model also estimates mass of the source in the range of 12–12.8 M_{\odot} . A monotonic evolution of the QPO frequency from higher to lower frequencies are observed, which is analogous to the QPO evolution in the declining phases of outbursts of a few transient BHCs (e.g., 2005 outburst of GRO J1655–40, 2010–11 outburst of GX 339–4, 2011 & 2011 outbursts of H 1743–322).

Mass is a crucial intrinsic parameter in astronomical sources, particularly in compact objects. Accurately determining the mass of the central BH in a binary system is essential for understanding accretion-ejection processes around it. However, dynamical measurements of BH masses are sometimes not possible due to the lack of information about the binary companion. In such cases, alternative methods are employed to estimate the mass of BHs. Some of these alternative methods include: the QPO frequency (ν)-photon index (Γ) correlation method (Shaposhnikov & Titarchuk 2007, 2009); the high-frequency QPO (HFQPO)-spin (a) correlation method (Motta et al. 2014); the inverse scaling relation with observed HFQPOs (Remillard & McClintock 2006); the QPO frequency evolution method (Iyer et al. 2015; Debnath et al. 2025); and the TCAF model-based spectral fitting method (Molla et al. 2016). The ν - Γ correlation method is widely used to estimate the masses of many neutron stars, black holes, and AGNs, while method based on TCAF model is also used to estimate the masses of more than 15 stellar mass BHCs.

Black hole spin is a fundamental parameter that influences both accretion and ejection processes. In X-ray binaries, spins are primarily estimated using two methods: the continuum-fitting method (CFM) and X-ray reflection spectroscopy (RS). Both techniques rely on fitting the observed X-ray spectra but are sensitive to different aspects of the accretion flow. The CFM (e.g. `kerrbb`) involves modeling the thermal X-ray emission from a geometrically thin, optically thick Keplerian accretion disk (see, e.g., Zhang et al. 1997; Shafee et al. 2006; Gou et al. 2010; Steiner et al. 2011), whereas the RS method models (e.g., `LAOR`, `relxill`)

the relativistically broadened iron K_α line and the associated reflection continuum (Laor 1991; Garcia et al. 2014; Mondal et al. 2016).

In this study, we analyze the evolution of the QPO frequency during the declining phase of the primary outburst of MAXI J1834-021 with the propagating oscillatory shock (POS) model. We also performed spectral study using combined NICER plus NuSTAR data with both phenomenological and physical models. The POS model fit as well as spectral study with the TCAF, **kerbb** models provides a good estimation of the mass of the BH. The **kerbb** model also estimates spin, distance, inclination angle of the source. The paper is organized as follows: §2 describes observations, data reduction, and analysis procedures. In §3, we present the results, while §4 discusses our findings and presents the conclusions.

2. OBSERVATION AND DATA ANALYSIS

2.1. Observations

NICER started to monitor MAXI J1834-021 roughly seven days after the announcement of the discovery by MAXI/GSC on March 06, 2023 (MJD 60009). The retrospective analysis of the MAXI/GSC suggests that the source was detected on February 05, 2023 (MJD 59980). In Paper-I, a detailed timing and spectral analysis has been made for 95 observations of the NICER/XTI instrument from March 07, 2023 (MJD = 60010.01) to October 04, 2023 (MJD = 60221.37). A monotonic evolution of the QPOs (2.12-0.12 Hz) are observed from March 09, 2023 (MJD = 60012) to April 28 (MJD = 60062.29). Here, we have adopted these data for further analysis using POS model. Additionally, we use one available observation from the NuSTAR/FPMA satellite instrument on March 10, 2023 (MJD = 60013.23) to perform a combined NICER plus NuSTAR spectral study over a broad energy band of 0.5–79 keV.

2.2. Data Reduction

We follow the standard data reduction procedures for the NICER and NuSTAR satellites.

2.2.1. NICER

NICER contains primary scientific payload, namely X-ray Timing Instrument (XTI; Gendreau et al. 2012). It is an independent satellite, attached as an external payload to the International Space Station. Its operating energy range is 0.2–12 keV with a time resolution of $\sim 0.1 \mu\text{s}$ and a spectral resolution of $\sim 85 \text{ eV}$ at 1 keV. For data analysis, we use the online platform SciServer¹ with HEASARC’s latest HEASoft package, version 6.34. The Level 1 data files are processed with the `nicerl2` script in the latest CALDB environment to obtain fully calibrated Level 2 event files, which are then screened for

non-X-ray events or bad data times. Light curves with 1 s and 0.01 s time bins in the energy bands 0.5–3 keV, 3–10 keV, and 0.5–10 keV are then extracted using the task `nicerl3-lc`. To obtain spectra in the default energy band, we use the task `nicerl3-spect` with SCORPEAN background model.

2.2.2. NuSTAR

NuSTAR archival data, downloaded from the web archive, are reduced using the latest NuSTAR data analysis software (NuSTARDAS, version 2.1.4a). Cleaned event files are produced using the `nupipeline` task with the latest calibration files. With the `XSELECT` task, a circular region of $60''$ centered at the source coordinates is chosen as the source region, while a circular region of the same radius, away from the source location, is chosen as the background region. The `nuprod-uct` task is then used to extract the spectrum, ARF, and RMF files. The extracted spectra are subsequently rebinned to have at least 20 counts per bin using the `GRPPHA` task.

2.3. Data Analysis

We use the task `lcstats` on NICER 1 s time-binned light curves to determine count rates in different energy bands. To study power density spectra (PDS), we analyze 0.01 s time-binned light curves in the 0.5–10 keV band. To determine the parameters (centroid frequency, full-width at half-maximum [FWHM], and power) of the QPOs, the PDS are fitted with a Lorentzian model using the XRONOS package of HEASoft.

The 0.5–10 keV NICER spectra are fitted with a combination of thermal disk blackbody (DBB) and power-law (PL) models in XSPEC (Arnaud 1996). To account for interstellar absorption, we use the TBabs model with the hydrogen column density (N_H) parameter set as free. The smedge model, with an edge energy of $\sim 0.81 \text{ keV}$, is used to compensate for instrumental features in the NICER spectra. For fitting combined NICER plus NuSTAR data, we use both phenomenological (DBB+PL) and theoretical (`nthComp`, TCAF, **kerbb**) models.

3. RESULTS

3.1. Low frequency QPOs and Their Evolution

In Paper-I, we studied detailed spectral and timing properties of MAXI J1834-021 using archival data of NICER/XTI for ~ 8 months from March 07, 2023 (MJD = 60010.01) to October 04, 2023 (MJD = 60221.37). From the evolution of temporal and spectral properties, our studied period of the 2023 active phase had been sub-divided into four phases. The evolution of outburst profiles in hard and soft X-ray bands, hardness ratios (HRs), low frequency QPOs, and spectral model fitted parameters, fluxes, accretion flow parameters, etc. confirms double ‘failed’ outbursts during 2023 active phase

¹ <https://www.sciserver.org>

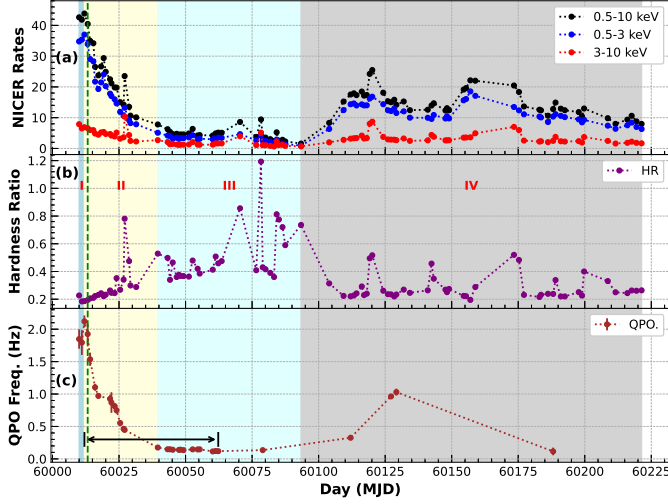


Figure 1. (a) Variation of NICER count rates in the soft X-ray (SXR; 0.5–3 keV), hard X-ray (HXR; 3–10 keV), and total X-ray (TXR; 0.5–10 keV) energy bands, shown in the top two panels. (b) Evolution of the hardness ratio (HR = HXR/SXR) is shown in the next panel. (c) In the bottom panel, the variation of the observed QPOs is shown. The shaded regions mark different phases of the outburst profile. The vertical green dashed-line corresponds to observation, whose detailed spectral study is made along with NUSTAR data. The both-side arrow mark the duration of the QPO evolution whose detailed study made with the POS model.

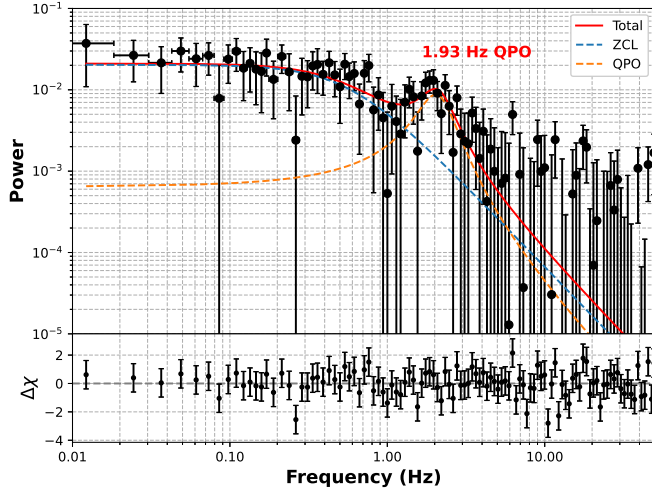


Figure 2. Fourier-transformed power density spectrum (PDS) of the 0.01 s time-binned 0.5–10 keV NICER light curve from March 10, 2023 (MJD 60013.23), fitted with combination of zero centric and QPO centric Lorentzian models. The model fit reveals a prominent QPO at 1.93 ± 0.16 Hz.

of the MAXI J1834-021. The Phases I-III corresponds to the primary outburst and Phase-IV is classified as mini-outburst. Furthermore, spectral analysis with the phenomenological (combined disk black body plus pow-

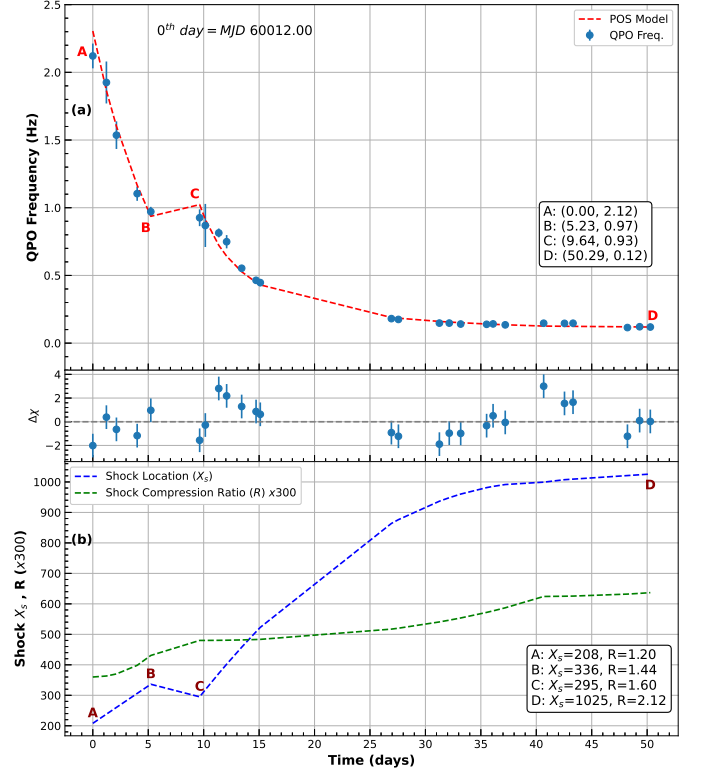


Figure 3. (a) Evolution of the observed QPO frequencies with time (in days) from March 9, 2023 (MJD 60012) to April 28, 2023 (MJD 60062.29), fitted with the POS model (dashed red curve). (b) Variation of the POS model-fitted shock location (X_s in Schwarzschild radius r_s) and shock compression ratio (R) are shown in the bottom panel. Points A-D mark the start, end, or major transition phases of the evolution.

erlaw or with only powerlaw) and physical (TCAF) models, and nature of QPOs confirms existence of harder spectral states throughout the 2023 active phase. The Phases I-III are classified as HS (rising), HIMS (declining) and HS (declining) respectively, and Phase-IV as undivided harder spectral state.

Low-frequency QPOs (LFQPOs) are observed throughout the outbursts. Most importantly, in Phases II & III, QPO frequencies are found to decrease monotonically from 2.12 Hz to 0.19 Hz within a period of ~ 50 days from March 09 to April 28, 2023 (MJD=60012-60062.29). This pattern of decreasing QPO frequencies is commonly observed in the declining harder states of transient BHCs (see Chakrabarti et al. 2008; Nandi et al. 2012; Debnath et al. 2013). In Fig. 1, we show variation of the soft X-ray (SXR; 0.5–3 keV), hard X-ray (HXR; 0.5–3 keV), total X-ray (TXR; 0.5–3 keV), HR (ratio between HXR with SXR), QPO frequencies. These data are adopted from Paper-I. This evolution of the QPO frequency is further studied here with the POS model. In Fig. 2, we show Fourier transformed power density spectrum (PDS) from March

10, 2023 (MJD 60013.23), fitted with a combination of one zero-centered and one QPO-centric Lorentzian models. It detects a prominent signature of QPO at 1.93 ± 0.16 Hz.

3.2. POS Model-Fitted QPO Evolution

The propagating oscillatory shock (POS) model (Chakrabarti et al. 2005, 2008) is the time-varying extension of the shock oscillation model (SOM Molteni et al. 1996; Ryu et al. 1997), which explains the origin of QPOs due to the oscillation of the shock. Shock oscillations occur due to heating and cooling effects within the hot Compton cloud, or CENBOL. As a result, the oscillation of the shock corresponds to the oscillatory variation in the size of the Compton cloud.

During the rising phase of transient BHCs, the oscillating shock moves inward due to an increased influx of Keplerian disk matter. Conversely, in the declining phase, the shock moves outward as the Keplerian disk matter supply decreases. According to the SOM, the QPO frequency (ν_{QPO}) follows an inverse relation with the shock location (X_s), given by: $\nu_{\text{QPO}} \sim X_s^{-3/2}$. Thus, in the rising phase of an outburst, we generally observe increasing QPO frequencies, whereas in the declining phase, the opposite trend is seen.

The sharp Type-C QPOs are associated with the resonance oscillation of the shock, when matter cooling time scales roughly matches with the infall time (t_{infall}) scales. So, according to (Chakrabarti et al. 2008),

$$\nu_{\text{QPO}} = \frac{\nu_{s0}}{t_{\text{infall}}} = \frac{c^3}{2GM_{\text{BH}}[RX_s(X_s - 1)^{1/2}]}, \quad (1)$$

where $\nu_{s0} = c/r_s = c^3/2GM_{\text{BH}} = 10^5/(M_{\text{BH}}/M_\odot)$ Hz is the inverse of the light crossing time of a black hole of mass M_{BH} and c is the velocity of light, $r_s = 2GM_{\text{BH}}/c^2$ is the Schwarzschild radius. Here $R(= \rho_+/\rho_-)$ is the shock compression ratio, i.e., ratio between the post- and pre-shock densities.

In the drifting or evolving shock scenario, $X_s = X_s(t)$ is time-dependent and can be expressed as

$$X_s(t) = X_{s0} \pm \frac{v(t)t}{r_s}, \quad (2)$$

where ‘−’ sign is used for inward and ‘+’ sign is used for receding shock motion. The shock velocity $v(t)$ may be accelerating, decelerating or constant and can be written as

$$v(t) = v_0 \pm v_a t, \quad (3)$$

where v_0 is the initial shock velocity and v_a is the velocity acceleration (‘+’)/deceleration (‘−’) term.

Generally during the rising phase of an outburst, the shock strength becomes weaker as the R decreases. On the day of the highest evolving QPO, it becomes even weaker, approaching $R \sim 1$. The opposite nature of R

can be seen in the declining phase of an outburst. The value of R generally follows the equation

$$\beta_s = \frac{1}{R} = \frac{1}{R_0} \pm \alpha t_d^2, \quad (4)$$

where the ‘+’ sign is used for the rising phase, and the ‘−’ sign is used for the declining phase. Here, R_0 represents the initial compression ratio, and α is the controlling factor that determines the rate of increase or decrease of R over time (t_d).

This model has been used to study the evolution of QPOs during the rising and/or declining phases of outbursts in several black hole candidates (BHCs), including GRO J1655-40 (Chakrabarti et al. 2005, 2008), GX 339-4 (Nandi et al. 2012), H 1743-322 (Debnath et al. 2013), XTE J1550-564 (Chakrabarti et al. 2009), and Swift J1727.8-1613 (Debnath et al. 2025). The model fit provides the instantaneous location, strength, and velocity of the oscillating shock. Iyer et al. (2015), Molla et al. (2016) and Debnath et al. (2025) successfully applied this model to estimate the mass of BHCs IGR J17091-3624, MAXI J1659-152, and Swift J1727.8-1613, respectively. These studies motivated us to investigate the monotonic evolution of QPO frequencies during Phases II and III of the current outburst of MAXI J1834-021.

After the initial rise in Phase-I, the QPO frequencies are found to monotonically decrease from 2.12 Hz (2023 March 9; MJD = 60012) to 0.12 Hz (2023 April 28; MJD = 60062.29). The monotonic evolution of the QPOs over this duration is quite similar to the evolution of QPOs during the declining phases of the 2005 outburst of GRO J1655-40 (Chakrabarti et al. 2008), the 2010-11 outburst of GX 339-4 (Nandi et al. 2012), and the 2010 & 2011 outbursts of H 1743-322 (Debnath et al. 2013). Similar to these earlier studies, the current evolution of the QPOs during the declining phase of the primary outburst is found to be well fitted with the POS model (see Fig. 3). The POS model-fitted QPO evolution, along with the variation of $\Delta\chi$, is shown in the top two panels of Fig. 3. The evolution of the POS model-fitted shock location (X_s) and compression ratio (R) is shown in the bottom panel of Fig. 3.

During around 50-day QPO evolution phase modeled by the POS model, the shock is found to move outward from $208 r_s$ to $1025 r_s$, with increasing shock strength. The compression ratio R changes from 1.20 to 2.12. The start, end, and significant transition phases of the evolution are marked as points A–D. In the initial branch AB (MJD = 60012–60017.23), spanning 5.23 days, a rapid decrease in the QPO frequency from 2.12 Hz to 0.97 Hz is observed. During this phase, X_s and R are found to vary from 208 – $336 r_s$, and 1.20 – 1.44 , respectively. After that, no QPOs are detected in branch BC (MJD = 60017.23–60021.63). Then, in branch CD (MJD = 60021.63–60062.29), spanning ~ 41 days, QPOs are found to decrease monotonically (from 0.93 to 0.20 Hz).

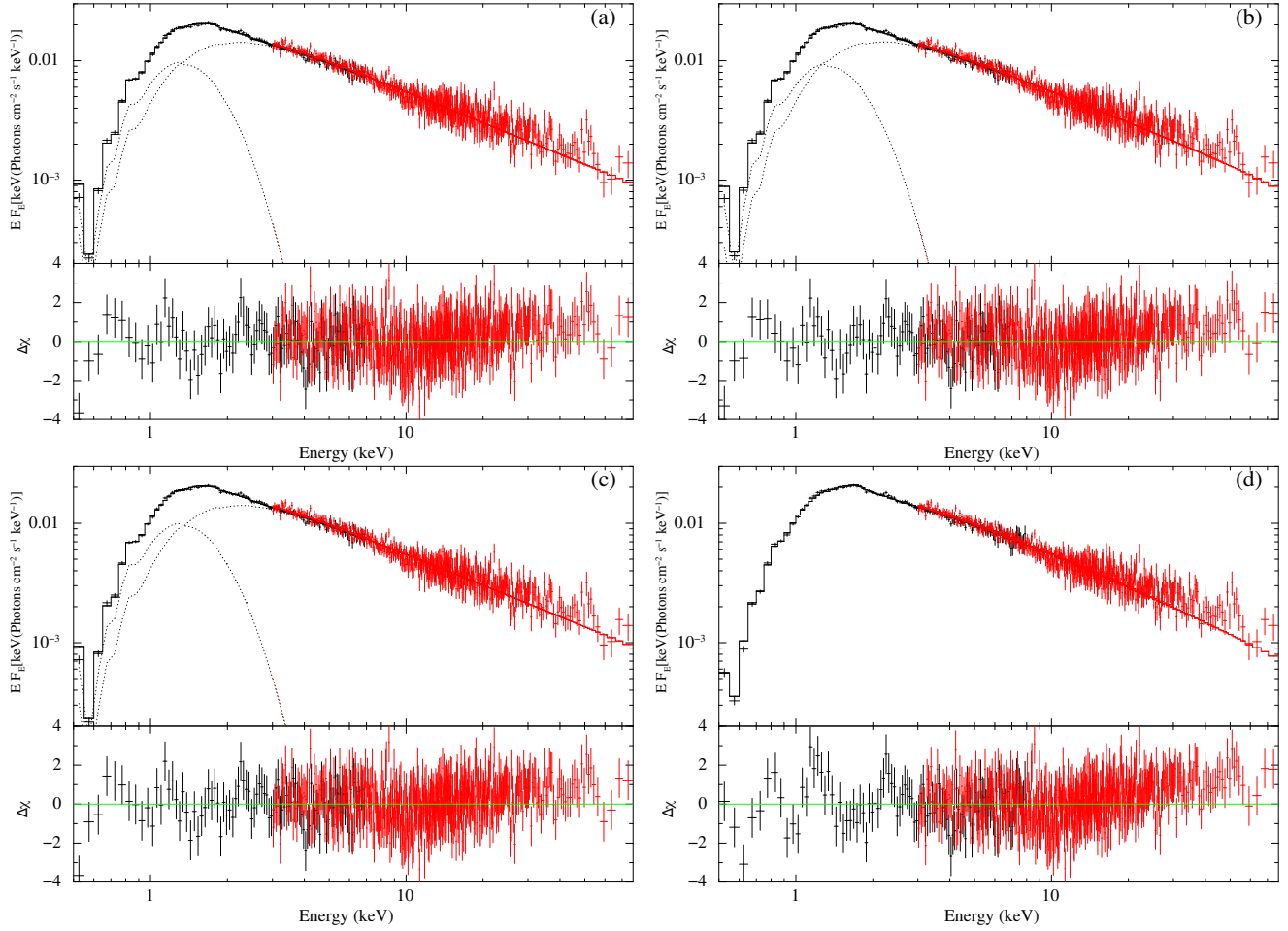


Figure 4. Combined NICER (0.5 – 8 keV) and NuSTAR (3 – 79 keV) spectrum of MAXI J1834-021 on March 10, 2023 (MJD 60013.23), fitted with different set of spectral models: (a) $constant \otimes tbabs \otimes smedge(diskbb + powerlaw)$, (b) $constant \otimes tbabs \otimes smedge(diskbb + nthComp)$, (c) $constant \otimes tbabs \otimes smedge(kerrbb + powerlaw)$, and (d) $constant \otimes tbabs \otimes smedge \otimes TCAF$.

During this phase, X_s and R vary from 295–1025 r_s and 1.6–2.12, respectively. Except in the late evolution phase, the shock velocity is observed to vary between 10–20 m/s.

From Eq. (1), it is evident that the black hole mass (M_{BH}) is an important parameter in the POS model. Thus, by fitting the POS model to the QPO frequency evolution, we are able to determine the mass of the newly discovered transient BHC MAXI J1834-021. From the best POS fit, we estimate the black hole mass to be $M_{BH} = 12.1 \pm 0.3 M_\odot$.

3.3. Combined NICER plus NuSTAR Spectral Study

To study the broadband nature of the source, we use the sole available NuSTAR observation along with the NICER observation from the same day. The combined NICER (0.5–8 keV) plus NuSTAR (3–79 keV) spectra from March 10 (MJD = 60013.23) are fitted with four sets of models: (i) $constant \otimes tbabs \otimes smedge(diskbb + powerlaw)$, (ii) $constant \otimes tbabs \otimes smedge(diskbb + nthComp)$, (iii) $constant \otimes tbabs \otimes smedge(kerrbb + powerlaw)$, and (iv) $constant \otimes tbabs \otimes smedge \otimes TCAF$

(see Fig. 4). The best-fit model parameters are listed in Table 1. Note, we have not fitted spectrum with the reflection based models (e.g., *pexrav*, *relxill*) as no prominent signature of the reflection feature were present in the data.

The model-fitted TBabs parameter N_H and *smedge* parameter *edgeE* are found to be consistent across all spectral fits. In sets (i) and (ii), the DBB temperatures T_{in} are found to be consistent, while in sets (i)–(iii), the PL photon indices remain consistent in a moderate value of 1.87 – 1.88. This values of Γ are generally seen in HIMS of transient BHCs (Nandi et al. 2012; Debnath et al. 2013). The sets (i) and (ii) confirms the presence of low temperature disk as T_{in} observed in between 0.30 – 0.35 keV.

The physical *kerrbb* model includes four source parameters (spin, mass, inclination, and distance) and one flow parameter (disk rate). So, the best-fitted *kerrbb* model provides us four important intrinsic source parameters such as spin $a = 0.13 \pm 0.09$, mass of the

BH $M_{\text{BH}} = 12.51 \pm 1.44 M_{\odot}$, disk inclination $i = 80^{\circ}.4 \pm 2^{\circ}.08$, and distance $D = 9.43 \pm 0.66$ kpc.

Similarly, the physical TCAF model yields accretion flow parameters: Keplerian disk rate $\dot{m}_d = 0.036 \pm 0.002 \dot{M}_{\text{Edd}}$, sub-Keplerian halo rate $\dot{m}_h = 0.589 \pm 0.010 \dot{M}_{\text{Edd}}$, shock location $X_s = 240 \pm 4.2 r_s$, and shock compression ratio $R = 1.13 \pm 0.06$. Additionally, it provides the BH mass as $M_{\text{BH}} = 12.41 \pm 0.13 M_{\odot}$. The presence of a higher halo accretion rate compared to the disk rate is consistent with the dominance of the PL flux over the DBB flux. The model-fitted X_s and R values are in agreement with the POS model-fitted QPO evolution values. Finally, the TCAF model-fitted M_{BH} is found to be consistent with the source mass values obtained from the POS and *kerbb* models.

3.4. MCMC Simulation and Contour Plots

The combined NICER and NuSTAR broadband (3–79 keV) spectral study on March 10 (MJD = 60013.23) using the *kerbb* model allowed us to estimate four important source parameters: spin (a), mass of the black hole (M_{BH}), disk inclination angle (i), and distance (D). To confirm these estimations, we performed a Markov Chain Monte Carlo (MCMC) simulation on the best-fitted spectrum in XSPEC². We employed the Goodman-Weare algorithm with 20 walkers and a total chain length of 200,000. The chain was initialized using a set of walkers drawn from a multi-dimensional Gaussian distribution with standard deviations 100 times the parameter uncertainties and means equal to the best-fit model parameters (see Table 1). The simulated results were saved as a FITS file.

We then used the publicly available *pyXspecCorner*³ code by Federico Garcia to generate corner plots showing contours between different model parameters using the MCMC-generated FITS file. In Fig. 5, we present the 1σ , 2σ , and 3σ confidence contours between the four intrinsic source parameters. Closed contours are observed at all three confidence levels for the following parameter pairs: a – M_{BH} , a – D , and D – M_{BH} . However, the 2σ and 3σ contours involving the inclination angle are not well closed. So, we can infer that within the 1σ confidence level, all four intrinsic parameters are reasonably well constrained.

In Fig. 5, the MCMC-derived best-fit model parameters along with their uncertainties are displayed. The intrinsic source parameters obtained from this method are: spin $a = 0.13^{+0.03}_{-0.02}$, disk inclination $i = 80^{\circ}.0^{+2.7}_{-6.0}$, black hole mass $M_{\text{BH}} = 12.3^{+1.1}_{-2.0} M_{\odot}$, and distance $D = 9.2^{+0.4}_{-0.9}$ kpc.

In Paper I, from a detailed spectral study of the outburst using the TCAF model, the black hole mass M_{BH}

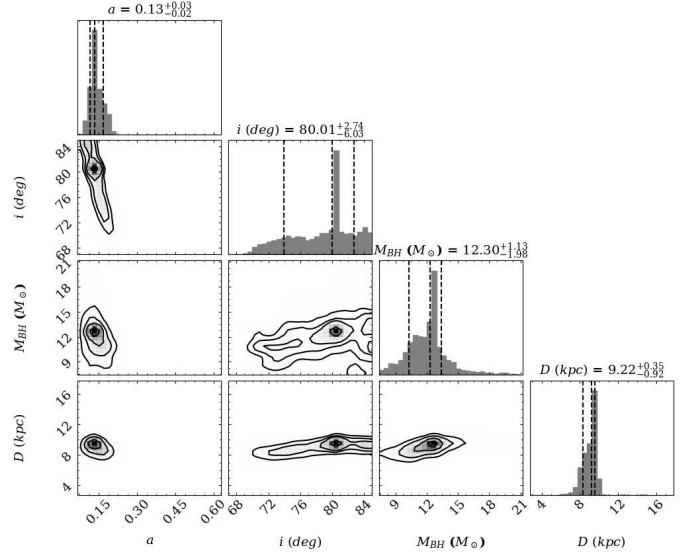


Figure 5. Contour plots (1, 2, and 3σ levels) between *kerbb* model fitted intrinsic source parameters such as spin (a), inclination angle (i), mass (M_{BH}), and distance (D). The Markov Chain Monte Carlo (MCMC) simulation generated fits file on best-fitted spectrum (using combined model set (iii): *constant* \otimes *tbabs* \otimes *smedge(kerrbb + powerlaw)*) has been used for the plots in *pyXspecCorner* code of Federico Garcia.

was estimated to lie within the range 12–12.8 M_{\odot} , with an average of 12.3 M_{\odot} , i.e., $12.3^{+0.5}_{-0.3} M_{\odot}$. Here, the mass estimates obtained using the POS, *kerbb*, and TCAF models are $12.1 \pm 0.3 M_{\odot}$, $12.3^{+1.1}_{-2.0} M_{\odot}$, and $12.4 \pm 0.1 M_{\odot}$, respectively. By combining these methods, we estimate the probable mass of MAXI J1834-021 to be $12.3^{+1.1}_{-2.0} M_{\odot}$.

3.5. Origin of the Observed QPO

The QPO frequency observed on the day of the combined NICER plus NuSTAR spectral analysis was 1.93 ± 0.16 Hz (see Fig. 2). The Lorentzian model fit yielded a line width (FWHM) of 0.538 ± 0.122 and a line normalization (power) of 0.0096 ± 0.0011 . The corresponding quality factor ($Q = \nu_{\text{QPO}}/\text{FWHM}$) and amplitude (in % rms, where $\text{rms} = (\pi/2) \times \text{Power} \times \text{FWHM}$) were found to be 3.58 and 9.02, respectively.

Assuming that type-C QPOs originate from the oscillation of a shock, Debnath et al. (2014) calculated the QPO frequencies for three BHCs using shock parameters obtained from TCAF model spectral fits. The close agreement between the theoretically predicted and the observed QPO frequencies strongly supported the hypothesis that shock oscillation was indeed responsible for the origin of the QPOs. This approach effectively predicts a temporal feature from spectral parameters. The same shock parameters—shock location (X_s) and compression ratio (R)—used to characterize the size of the Compton cloud and the matter densities in the pre-

² <https://heasarc.gsfc.nasa.gov/xanadu/xspec/manual/node43.html>

³ <https://github.com/garciafederico/pyXspecCorner>

Table 1. Spectral results of combined NICER (0.5-8 keV) and *NuSTAR* (3-79 keV) data on March 10, 2023

TBABS⊗SMEDGE(DISKBB+POWERLAW)			TBABS⊗SMEDGE(DISKBB+NTHCOMP)		
Tbabs	N_H ($\times 10^{22}$ cm $^{-2}$)	0.78 ± 0.02	Tbabs	N_H ($\times 10^{22}$ cm $^{-2}$)	0.72 ± 0.02
diskbb	kT_{in} (keV)	0.30 ± 0.02	diskbb	kT_{in} (keV)	0.35 ± 0.02
	Norm	1180 ± 32		Norm	364 ± 15
powerlaw	Γ	1.87 ± 0.01	nthComp	Γ	1.88 ± 0.04
	Norm	0.04 ± 0.001		kT_e (keV)	999.5
	χ^2/DOF	$617/578$		kT_{bb}	0.15
F_{DBB}	(erg cm $^{-2}$ s $^{-1}$)	1.75×10^{-11}		Norm	3.79
F_{PL}	(erg cm $^{-2}$ s $^{-1}$)	3.45×10^{-10}		χ^2/DOF	$620/576$
			F_{DBB}	(erg cm $^{-2}$ s $^{-1}$)	1.70×10^{-11}
			$F_{nthComp}$	(erg cm $^{-2}$ s $^{-1}$)	3.42×10^{-10}
TBABS⊗SMEDGE(KERRBB + POWERLAW)			TBABS⊗SMEDGE⊗TCAF		
Tbabs	N_H ($\times 10^{22}$ cm $^{-2}$)	0.81 ± 0.09	Tbabs	N_H ($\times 10^{22}$ cm $^{-2}$)	0.89 ± 0.05
kerrbb	spin a	0.13 ± 0.09	TCAF	\dot{m}_d (\dot{M}_{Edd})	0.036 ± 0.002
	Inclination i (deg)	80.4 ± 2.08		\dot{m}_h (\dot{M}_{Edd})	0.589 ± 0.010
	M_{BH} (M_\odot)	12.51 ± 1.44		M_{BH} (M_\odot)	12.41 ± 0.13
	\dot{m}_d (10^{18} g/s)	0.09 ± 0.02		X_s (r_s)	240 ± 4.2
	Distance D (kpc)	9.43 ± 0.66		R	1.13 ± 0.06
	Norm	1.14 ± 0.16		Norm	4.81 ± 0.05
powerlaw	Γ	1.87 ± 0.01		χ^2/DOF	$695/587$
	Norm	0.04 ± 0.001	F_{TCAF}	(erg cm $^{-2}$ s $^{-1}$)	3.47×10^{-10}
	χ^2/DOF	$615/574$			
F_{kerrbb}	(erg cm $^{-2}$ s $^{-1}$)	1.83×10^{-11}			
F_{PL}	(erg cm $^{-2}$ s $^{-1}$)	3.04×10^{-10}			

The smedge model parameter $edgeE$ is found to be at ~ 0.81 keV for all four set of models.

shock and post-shock regions are also used to calculate QPO properties via the POS model. Using the TCAF model-fitted values of M_{BH} , X_s , and R in Eq. (1), we obtain a theoretical QPO frequency of 1.92 ± 0.16 Hz. The consistency between this calculated and observed ν_{QPO} further confirms shock oscillation as the likely origin of the detected QPO in our studied observation of MAXI J1834-021.

4. DISCUSSION AND CONCLUDING REMARKS

The Galactic transient BHC MAXI J1834-021 was detected on February 05, 2023 (MJD = 59980) by MAXI/GSC and its X-ray activity was continued for the next ~ 10 months. Due to almost one month delay in the report of the discovery (March 06, 2023), we have missed initial rising phase data of the source. In Paper-I, we studied the spectral and timing properties of the source during the initial ~ 8 months (2023 March 7 to October 4; MJD = 60010.01-60221.37) to understand accretion flow dynamics of the source during its 2023 active phase. From the daily variations in X-ray intensities in the soft (0.5–3 keV, SXR), hard (3–10 keV, HXR), and total (0.5–10 keV, TXR) energy bands, nature of the observed QPOs, and spectral fitted param-

eters, fluxes, etc. reveals four distinct stages during the outburst (see shaded regions of Fig. 1). The Phases I–III are classified as primary and Phase-IV is classified as mini-outburst. Spectral studies were made with both phenomenological (combined disk blackbody plus powerlaw or only powerlaw) and physical (TCAF) models. The TCAF model also estimated mass of the source.

In Phases II & III of the outburst i.e., in the declining phase of the primary outburst, a monotonic evolution of the QPO frequency from 2.12 to 0.20 Hz (in between MJD = 60012–60062.29) is observed. Here, To understand the nature of this QPO evolution from a physical point of view, we studied it using the POS model (see Fig. 3). The POS model fit allowed us to determine the physical flow parameters such as instantaneous location of the shock, compression ratio, velocity, etc. The shock is found to recede from 208–1025 r_s with a slowly increasing strength. The best-fitted POS model also enabled us to estimate the mass of the BH, as M_{BH} is an essential parameter of the model (see Eq. 1). The mass of the BH is obtained as $M_{BH} = 12.1 \pm 0.3 M_\odot$. This is consistent with the mass range (12 – 12.8 M_\odot) of the source reported in Paper-I.

The spectral study throughout the 2023 active phase was done using 0.5 – 10 keV NICER data in Paper-I. The study confirms that the presence of harder (HS and HIMS) spectral states with a dominance of nonthermal fluxes from ‘hot’ Compton cloud i.e., sub-Keplerian halo accretion rate over the disk rate. Here, we make an attempt to study broadband nature (in 0.5 – 79 keV) of the source using combined NICER (0.5 – 10 keV) plus NuSTAR (3 – 79 keV) data from March 10, 2023 (see, Fig. 4 and Table 1). The spectrum has been studied with four different set of phenomenological as well as physical models. The combined DBB plus PL, and combined DBB plus nthComp infers presence of cooler disk with temperature T_{in} in between 0.30 – 0.35 keV. The TCAF model fit also tells about the lower Keplerian disk accretion rate which is supposed to the origin of the DBB photons, compared to the sub-Keplerian halo rate. The *kerrbb* model also finds lower disk rate. The photon indices obtained from DBB+PL, DBB+nthComp, and *kerrbb*+PL model fits are found to be consistent with values in a constant range of 1.87 – 1.88. This Γ values are generally seen in HIMS of transient stellar mass BHs.

The broadband analysis using the physical TCAF and *kerrbb* models allowed us to estimate four intrinsic source parameters: mass, spin, disk inclination angle, and distance. To validate the intrinsic parameters obtained from the *kerrbb* model, we performed an MCMC simulation in XSPEC. Confidence contours were plotted using the MCMC-generated fits file and the publicly available *pyXspecCorner* code. These contours provided constraints on the fitted parameter values and their uncertainties. From this method, we estimated the spin $a = 0.13^{+0.03}_{-0.02}$, disk inclination $i = 80^\circ.0^{+2.7}_{-6.0}$, mass $M_{BH} = 12.3^{+1.1}_{-2.0} M_\odot$, and distance $D = 9.2^{+0.4}_{-0.9}$ kpc.

Combining the M_{BH} estimates from TCAF model fits in Paper-I ($12\text{--}12.8 M_\odot$, or $12.3^{+0.5}_{-0.3} M_\odot$), the present TCAF fit ($12.41 \pm 0.13 M_\odot$), the POS model fit ($12.1 \pm 0.3 M_\odot$), and the above MCMC-simulated *kerrbb* results, we infer the probable mass of MAXI J1834–021 as $12.3^{+1.1}_{-2.0} M_\odot$. The estimated low spin ($a = 0.13^{+0.03}_{-0.02}$) places MAXI J1834–021 among a few sources with spins below 0.3, such as A0620–00 ($a = 0.12 \pm 0.19$, Gou et al. 2010), H1743–322 ($a = 0.2 \pm 0.3$, Steiner et al. 2011), and LMC X-3 ($a = 0.25^{+0.20}_{-0.29}$, Steiner et al. 2014). The high inclination angle ($i = 80^\circ.0^{+2.74}_{-6.03}$) makes this source a suitable candidate for soft-lag studies (see, e.g., Dutta & Chakrabarti 2016). A detailed study of the lag properties will be presented elsewhere.

A prominent QPO of 1.93 ± 0.16 Hz is observed in NICER data on March 10, 2023, whose detailed spectral study has been done in this paper (see inset in Fig. 1). To find origin of this QPO, we followed method as described in Debnath et al. (2014). The frequency of the primary QPO is being calculated from the TCAF model fitted shock parameters (X_s and R). If the shock oscil-

lation being the origin of the observed QPO, the calculated QPO should match with the observed one. Here, using TCAF model fitted X_s , R , and M_{BH} in Eq. (1), we calculated theoretical ν_{ThQPO} as 1.92 ± 0.16 , which matches with the observed ν_{QPO} . This actually confirm oscillation of the shock as the origin of the observed QPO on March 10, 2023.

A brief summary of our findings in this *paper* is as follows:

- i) The entire period of the 2023 activity of MAXI J1834-021 exhibits variations in soft (SXR; 0.5–3 keV), hard (HXR; 3–10 keV), and total (TXR; 0.5–10 keV) X-ray count rates, QPO frequencies, etc., which classify the event into four phases of a double outburst.
- ii) Strong signatures of LFQPOs are observed throughout the outburst. The monotonic evolution of QPOs during the declining phase of the primary outburst is further studied with the POS model. A receding shock with slowly increasing strength is found. The POS model also estimated the mass of the BH as $12.1 \pm 0.3 M_\odot$.
- iii) The combined NICER plus NuSTAR spectral analysis on 2023 March 10, in a broad energy band with four sets of models not only allowed us to understand the nature of the source from a physical perspective but also estimates the intrinsic source parameters. The source was found in hard-intermediate spectral state with higher dominance of non-thermal photons.
- iv) The spectral fit with the physical *kerrbb* model estimates the mass, spin, distance, and inclination angle as $M_{BH} = 12.3^{+1.1}_{-2.0} M_\odot$, $a = 0.13^{+0.03}_{-0.02}$, $D = 9.2^{+0.4}_{-0.9}$ kpc, and $i = 80^\circ.0^{+2.7}_{-6.0}$, respectively.
- v) The spectral fit with the TCAF model finds a higher halo accretion rate (\dot{m}_h) compared to the disk rate (\dot{m}_d). The shock parameters ($X_s = 240 \pm 4.2$ and $R = 1.13 \pm 0.06$) signify the presence of a large Compton cloud with moderate strength. The model also estimates the mass of the source as $12.4 \pm 0.1 M_\odot$.
- vi) Combining the estimated M_{BH} values from the POS, *kerrbb*, and TCAF models, we predict the most probable mass of MAXI J1834–021 as $12.3^{+1.1}_{-2.0} M_\odot$, or within the range of $11.2\text{--}14.3 M_\odot$.
- vii) The match between the theoretically estimated QPO frequency from the TCAF model-fitted shock parameters and the observed one confirms shock oscillation as the origin of the prominent 1.93 ± 0.16 Hz QPO on March 10, 2023.

ACKNOWLEDGEMENTS

This work made use of NICER/XTI and NuSTAR/FPMA data supplied by the High Energy Astrophysics Science Archive Research Center (HEASARC)

archive. D.D. acknowledge the visiting research grant of National Tsing Hua University, Taiwan (NSTC NSTC 113-2811-M-007-010). H.-K. C. is supported by NSTC of Taiwan under grant NSTC 113-2112-M-007-020.

REFERENCES

- Belloni, T., Homan, J., Casella, P., et al., 2005, *A&A*, 440, 207
- Bright, J., Fender, R., Green, D., et al., 2023, *ATel*, 15939, 1
- Casella, P., Belloni, T., & Stella, L., 2005, *ApJ*, 629, 403
- Chakrabarti, S. K. & Titarchuk, L. G., 1995, *ApJ*, 455, 623
- Chakrabarti, S.K., Nandi, A., Debnath, D. Sarkar, R. & Datta, B.G., 2005, *Ind. J. Phys.*, 78B, 1
- Chakrabarti, S.K., Debnath, D., Nandi, A., Pal, P. S., 2008, *A&A* 489, L41
- Chakrabarti, S. K., Dutta, B. G., Pal, P. S., 2009, *MNRAS*, 394, 1463
- Chakrabarti, S.K., Mondal, S., & Debnath, D., 2015, *MNRAS*, 452, 3451
- Debnath, D., Chakrabarti, S. K., & Nandi, A., 2013, *AdSpR*, 52, 2143
- Debnath, D., Chakrabarti, S.K., & Mondal, S., 2014, *MNRAS*, 440, L121
- Debnath, D., Mondal, S., & Chakrabarti, S.K., 2015, *MNRAS*, 447, 1984
- Debnath, D., Chang, H. K., Nath, S. K., Titarchuk, L., 2025, *ApJ* (in communication) (arXiv:2504.16391)
- Debnath, D., & Chang, H. K., 2025, *ApJ* (in communication) (Paper-I) (arXiv:2504.16398)
- Dutta, B. J., & Chakrabarti, S. K. 2016, *ApJ*, 828, 101
- Garcia, J., Dauser, T., Lohfink, A., et al., 2014, *ApJ*, 782, 76
- Gendreau, K. C., Arzoumanian, Z., & Okajima, T. 2012, *Proc. SPIE*, 8443, 844313
- Gou, L., McClintock, J. E., Steiner, J. F., et al., 2010, *ApJ*, 718, L122
- Homan, J., Gendreau, K., Arzoumanian, Z., et al., 2023, *ATel*, 15951, 1
- Iyer, N., Nandi, A., & Mandal, S., 2015, *ApJ*, 807, 108
- Kennea, J. A., Page, K. L., Negoro, H., 2023, *ATel*, 15932, 1
- Li, Li-Xin, Zimmerman, E. R., Narayan, R., McClintock, J. E., 2005, *ApJS*, 157, 335
- Laor, A., 1991, *ApJ*, J. 376, 90
- Magdziarz, P. & Zdziarski, A., A., 1995, *MNRAS*, 273, 837
- Mondal, S., Chakrabarti, S. K., & Debnath, D., 2016, *Ap&SS*, 361, 309
- Marino, A., Borghese, A., Coti Zelati, F., et al., 2023, *ATel*, 15946, 1
- Molla A. A., Debnath D., Chakrabarti S. K., et al., 2016, *MNRAS*, 460,3163
- Molteni D., Sponholz H., Chakrabarti S. K., 1996, *ApJ*, 457, 805
- Motta, S. E., Muñoz-Darias, T., Sanna, A., 2014, *MNRAS*, 439, L65
- Nandi, A., Debnath, D., & Mandal, S., et al., 2012, *A&A*, 542, 56
- Negoro, H., Nakajima, M., Kobayashi, K., et al., 2023, *ATel*, 15929, 1
- Remillard, R. A., & McClintock, J. E., 2006, *ARA&A*, 44, 49
- Ryu D., Chakrabarti S. K., Molteni D., 1997, *ApJ*, 474, 378
- Saikia, P., Russell, D. M., Alabarta, K., et al., 2023, *ATel*, 15940, 1
- Shafee, R., McClintock, J. E., Narayan, R., et al., 2006, *ApJ*, 636, L113
- Shaposhnikov, N., & Titarchuk, L. 2007, *ApJ*, 663, 445
- Shaposhnikov, N., & Titarchuk, L. 2009, *ApJ*, 699, 453
- Steiner, J. F., McClintock, J. E., Reid, M. J., 2011, *ApJ*, 745, L7
- Steiner, J. F., McClintock, J. E., Orosz, J. A., et al., 2014, *ApJ*, 793, L29
- Zdziarski, A. A., Johnson, W. N., & Magdziarz, P., 1996, *MNRAS*, 283, 193
- Zhang, S. N., et al., 1997, *ApJ*, 482, L155
- Zycki, P. T., Done, C., & Smith, D. A., 1999, *MNRAS*, 309, 561